Spectral Effects in Albedo and Rearside Irradiance Measurement for Bifacial Performance Estimation

Preprint

Michael Gostein,[1] Bill Marion,[2] and Bill Stueve[1]

1 Atonometrics
2 National Renewable Energy Laboratory

Presented at the 47th IEEE Photovoltaic Specialists Conference (PVSC 47)
June 15 – August 21, 2020

NREL is a national laboratory of the U.S. Department of Energy
Office of Energy Efficiency & Renewable Energy
Operated by the Alliance for Sustainable Energy, LLC

This report is available at no cost from the National Renewable Energy Laboratory (NREL) at www.nrel.gov/publications.

Contract No. DE-AC36-08GO28308

Conference Paper
NREL/CP-5K00-75927
August 2020

Spectral Effects in Albedo and Rearside Irradiance Measurement for Bifacial Performance Estimation

Preprint

Michael Gostein,[1] Bill Marion,[2] and Bill Stueve[1]

1 Atonometrics
2 National Renewable Energy Laboratory

Suggested Citation
Gostein, Michael, Bill Marion, and Bill Stueve. 2020. *Spectral Effects in Albedo and Rearside Irradiance Measurement for Bifacial Performance Estimation: Preprint*. Golden, CO: National Renewable Energy Laboratory. NREL/ CP-5K00-75927.
https://www.nrel.gov/docs/fy20osti/75927.pdf.

Conference Paper
NREL/CP-5K00-75927
August 2020

National Renewable Energy Laboratory
15013 Denver West Parkway
Golden, CO 80401
303-275-3000 • www.nrel.gov

NOTICE

This work was authored in part by the National Renewable Energy Laboratory, operated by Alliance for Sustainable Energy, LLC, for the U.S. Department of Energy (DOE) under Contract No. DE-AC36-08GO28308. Funding provided by U.S. Department of Energy Office of Energy Efficiency and Renewable Energy Solar Energy Technologies Office. The views expressed herein do not necessarily represent the views of the DOE or the U.S. Government. The U.S. Government retains and the publisher, by accepting the article for publication, acknowledges that the U.S. Government retains a nonexclusive, paid-up, irrevocable, worldwide license to publish or reproduce the published form of this work, or allow others to do so, for U.S. Government purposes.

Cover Photos by Dennis Schroeder: (clockwise, left to right) NREL 51934, NREL 45897, NREL 42160, NREL 45891, NREL 48097, NREL 46526.

Spectral Effects in Albedo and Rearside Irradiance Measurement for Bifacial Performance Estimation

Michael Gostein
Atonometrics
Austin, USA

Bill Marion
National Renewable Energy Laboratory
Golden, USA

Bill Stueve
Atonometrics
Austin, USA

***Abstract*—We investigate the impact of spectral dependence of ground surface reflectivity on albedo and rearside irradiance measurements necessary for bifacial photovoltaic (PV) module performance estimation and monitoring. Because PV modules are spectrally selective, albedo and irradiance measurements performed with common irradiance sensors may require spectral mismatch corrections when used for performance prediction. We investigate via simulation the differences in spectrally responsive albedo measured with thermopile pyranometers and crystalline silicon PV reference cells in comparison to a typical crystalline-silicon bifacial PV module. Simulations are performed for nine different representative ground surface materials using simulated solar spectra together with spectral reflectivity data distributed with the SMARTS simulation software. For the materials considered, the results show that albedo spectral mismatch relative to the bifacial module is distributed over a range of $\pm$9.2% for thermopile pyranometers versus only $\pm$3.7% for a typical PV reference cell. We consider the impact of this spectrally-responsive albedo mismatch on bifacial PV module rearside irradiance measurements. Using synthesized rearside spectral irradiance distributions, we find that for the nine different ground surface materials the predicted rearside irradiance measurement deviates from the effective irradiance observed by the PV module by on the order of 16.5 W/m^2 for the pyranometer and 3.6 W/m^2 for the PV reference cell. We discuss the implications for bifacial albedo and irradiance measurement.**

***Index Terms*—photovoltaic (PV) systems, bifacial, resource assessment, pyranometer, reference cell**

I. Introduction

With the rapid adoption of bifacial photovoltaic (PV) modules the measurement of albedo and bifacial rearside irradiance has become of increasing importance, for both resource assessment on prospective sites and performance monitoring of built systems. However, best practices are not yet completely defined and industry participants have many questions about the impact of different measurement choices.

Among the areas of uncertainty is the importance of spectral response of irradiance sensors relative to the spectral response of PV modules. The spectral reflectivity of ground surfaces can significantly alter the spectrum of ground-reflected radiation versus that of downwelling radiation from the sky, and it is well known that this has an important influence on bifacial PV performance [1]. However, there are few reports that provide quantitative assessments of the spectral mismatch of albedo and irradiance measurements versus bifacial PV modules for different irradiance sensor types.

Here we will present a summary of bifacial module spectral mismatch of albedo and irradiance measurement using both thermopile pyranometers, which are broadband sensors, and PV reference cells, which have spectral selectivity similar to that of PV modules, based on simulations similar to those in [2] [3]. Our aim is to provide relevant examples of the uncertainty of effective albedo and irradiance for both types of irradiance sensors in typical situations.

II. Spectrally Responsive Albedo

A. Definitions

In the context of PV performance estimation, albedo is the reflectivity of a particular ground material for incident solar radiation. For simplicity it is common to consider the albedo of a ground surface to be a constant, however in fact it depends on wavelength as well as angle. Therefore the spectral response of a measuring device or PV module affects the amount of ground-reflected radiation that is detected or available for PV power generation.

Following [4] [5] we define the spectrally responsive albedo as

$$\rho_S = \frac{\int R(\lambda) SR(\lambda) G(\lambda) d\lambda}{\int SR(\lambda) G(\lambda) d\lambda} \quad (1)$$

where $G(\lambda)$ is the spectral irradiance of incident solar radiation in a horizontal plane at wavelength λ, $SR(\lambda)$ is the spectral response of the measurement device or PV module, and $R(\lambda)$ is the spectral reflectivity of the ground surface. The denominator represents downwelling incident solar radiation and the numerator represents ground-reflected upwelling radiation. The subscript S distinguishes the spectrally responsive albedo from the total albedo neglecting spectral response. In (1) we neglect angular responsivity, but comment on its importance below.

Using (1) we define spectrally responsive albedos ρ_S^{Pyr}, $\rho_S^{Refcell}$, and ρ_S^{Module} for a thermopile pyranometer, PV reference cell, and PV module, respectively, by using the spectral response of each device for $SR(\lambda)$, with the device indicated in the superscript. In the case of a bifacial PV module, $SR(\lambda)$ in the numerator and denominator could be different, as discussed below.

Our aim in albedo measurement is to estimate the performance of a PV system. Accordingly, we define a spectral

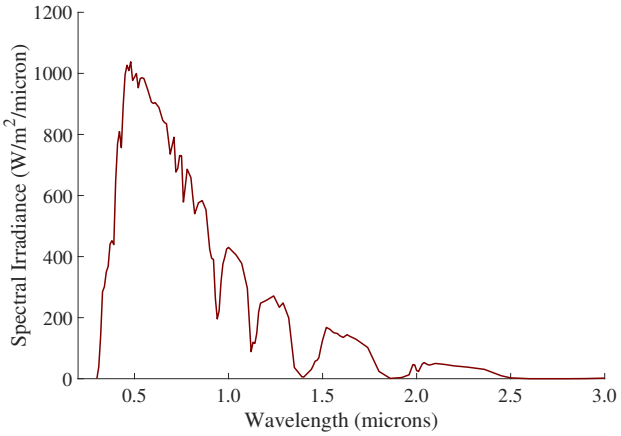

Fig. 1. Incident horizontal spectral irradiance for albedo simulation.

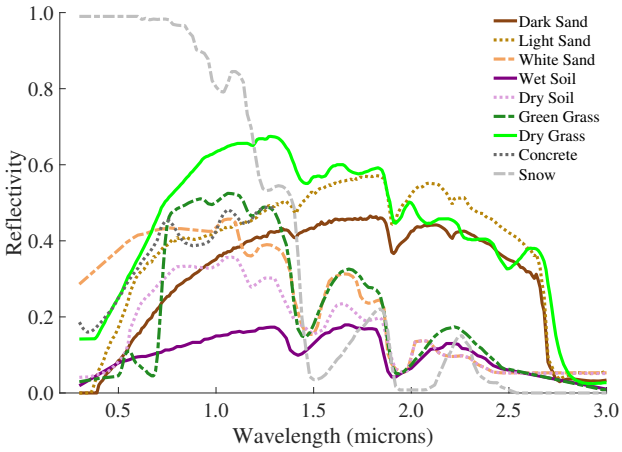

Fig. 2. Spectral reflectance of nine ground surfaces from SMARTS database.

mismatch factor versus the PV module for albedo measured by each of the irradiance sensors as

$$M^{Pyr} = \rho_S^{Pyr}/\rho_S^{Module} \tag{2}$$

and

$$M^{Refcell} = \rho_S^{Refcell}/\rho_S^{Module} \tag{3}$$

B. Simulations

For simulations on spectrally responsive albedo, we used the Bird spectral model [6] to generate a representative clear-sky spectral irradiance distribution $G(\lambda)$ corresponding to the standard reporting conditions set forth for the IEC 60904-3 reference spectrum, with the exception that the receiving plane was chosen to be horizontal, rather than at 37° tilt, in order to represent global horizontal radiation. Fig. 1 shows the simulated spectrum.

We performed simulations for nine different ground surface materials using spectral reflectivity files included in the SMARTS simulation software [7] to generate $R(\lambda)$ for each material. Spectral reflectivities for each of the materials are shown in Fig. 2. Several of the curves were linearly extended down to 0.3 microns when the data supplied by SMARTS ended at 0.5 microns. Note that many of the materials exhibit higher reflectance in the infrared region above 1.2 microns (the band edge for silicon PV response) and reduced reflectance below approximately 0.6 microns.

Fig. 3 shows the normalized spectral response curves used for the simulations. For the spectral response of the thermopile pyranometer, $SR^{Pyr}(\lambda)$, we used [8]. For $SR^{Refcell}(\lambda)$, we used a spectral response measurement performed at the National Renewable Energy Laboratory (NREL) for a representative Atonometrics mono-crystalline silicon PV reference cell. For the PV module we obtained representative spectral responses from the front and rear sides of a bifacial PV module by averaging measured spectral response curves for the six commercially available bifacial PV modules reported in [9]. While Fig. 3 shows normalized curves, each of the $SR(\lambda)$ functions includes a calibration scaling constant chosen such that $\int SR(\lambda)G_0(\lambda)d\lambda = 1000$ W/m^2, where $G_0(\lambda)$ is the IEC

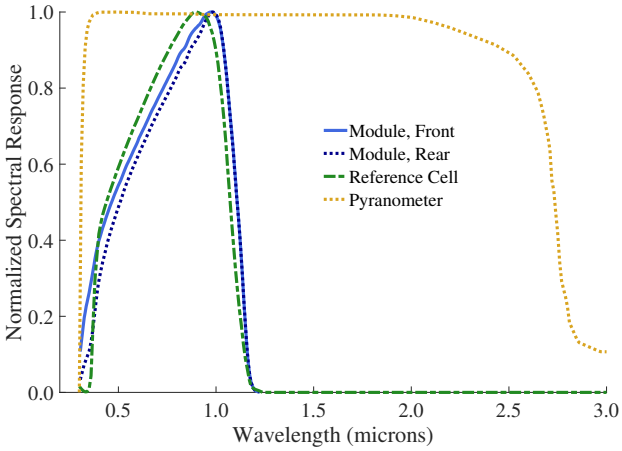

Fig. 3. Normalized spectral responses of irradiance sensors and module.

60904-3 reference spectral irradiance for standard reporting conditions.

For thermopile pyranometers and reference cells the $SR(\lambda)$ we use in the numerator and denominator of (1) are equal, since identical sensors would be used facing up and down. However for the bifacial module the $SR(\lambda)$ in the numerator and denominator are the slightly different spectral responses of the front and rear of the module, respectively.

C. Results

Fig. 4 shows the simulation results for the spectrally responsive albedo of the thermopile pyranometer, PV reference cell, and PV module for each of the nine ground surfaces. Note that the albedo varies greatly depending on the specific properties of the material – for example dark, light, or white sand; wet or dry soil; green or dry grass.

Fig. 5 shows spectral mismatch factors for the thermopile pyranometer and PV reference cell relative to the PV module, M^{Pyr} and $M^{Refcell}$ calculated by (2) and (3). M^{Pyr} is higher when the ground surface has a high reflectivity in the infrared beyond the silicon band edge (e.g. dark sand) and generally lower when the ground surface has relatively lower

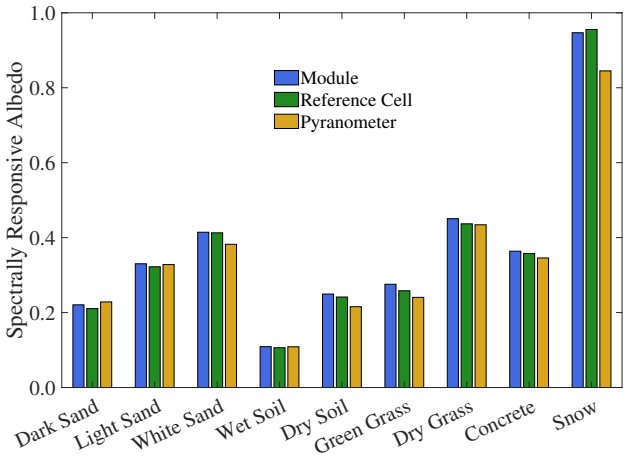

Fig. 4. Results of simulation for spectrally responsive albedo.

reflectivity in the infrared (e.g. white sand, snow). $M^{Refcell}$ follows a roughly opposite trend, with smaller variation. For the nine materials simulated, the spectral mismatch factor for the pyranometer ranges from 0.86 to 1.04 versus 0.94 to 1.01 for the PV reference cell. The range of variation for the reference cell is smaller due to its spectral response being similar to that of the module.

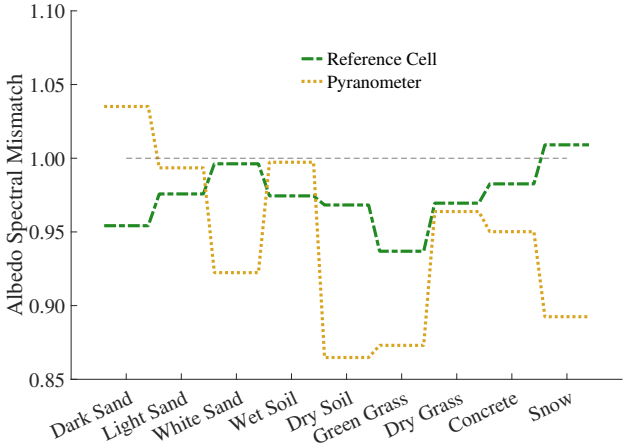

Fig. 5. Albedo spectral mismatch versus module.

III. Rearside Irradiance

While albedo values are used for bifacial PV performance estimation, for performance monitoring of fielded bifacial PV modules it is desirable to directly measure the rearside irradiance. However, the different spectal responsivities of irradiance sensors and PV modules can yield differences between measured irradiance and effective irradiance available to the module.

To estimate the magnitude of these variations, we have simulated the rearside spectral irradiance distribution for representative conditions, using an approach guided by [10]. As in [10], we consider a bifacial PV module at the standard reporting conditions of IEC 60904-3 (including 37° module tilt, air mass 1.5, and other standard conditions) and estimate the rear spectral irradiance based on direct and diffuse components of the incident front spectral irradiance and their reflectance from the ground surface onto the rear of the module, as well as the illumination of the module rearside with diffuse irradiance from the sky. We generate the incident front direct and diffuse spectra using the Bird model [6]. We synthesize the rearside spectral irradiance distribution according to

$$G_{rear}(\lambda) = a \cdot R(\lambda) \cdot G_0^{DNI}(\lambda) + (b \cdot R(\lambda) + c) \cdot G_0^{Dif}(\lambda) \quad (4)$$

where $R(\lambda)$ is the ground surface spectral reflectance as before and $G_0^{DNI}(\lambda)$ and $G_0^{Dif}(\lambda)$ are the direct normal and diffuse spectral irradiance distributions calculated with the Bird model for standard reporting conditions. The constants a, b, and c could be determined by a view-factor or configuration model approach as in [10] [11] for the specific geometry of the bifacial system and would vary with tilt, sun position, etc. However since we are considering only a single representative case, for simplicity we assign values $a = 0.4$, $b = 0.4$, $c = (1+cos(180° - 37°))/2 = 0.1$, which produce reasonable results similar to [10]. This allows us to compare the effect of different ground surface materials with different $R(\lambda)$.

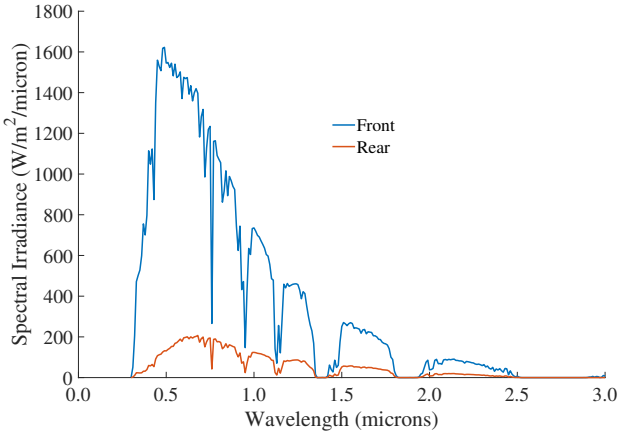

Fig. 6. Simulated rear spectral irradiance for ground material "light sand" compared to standard front spectral irradiance.

As an example, Fig. 6 illustrates our simulated rearside spectral irradiance using $R(\lambda)$ for "light sand," compared with the incident front side spectral irradiance corresponding to standard reporting conditions. Note that the peak of the rearside spectral irradiance is shifted to longer wavelengths compared to the incident front spectrum, due to the ground surface.

To compute the irradiance that would be measured by an irradiance sensor mounted in the module's rear plane or the equivalent rearside irradiance available to the module, we calculate

$$E_{rear} = \int G_{rear}(\lambda) \cdot SR(\lambda) \cdot d\lambda \quad (5)$$

using $SR(\lambda)$ functions for the module rear, pyranometer, and PV reference cell as shown in Fig. 3. Fig. 7 and Table I show

these results. For light sand, the material used in [10], our rear irradiance value of 140 W/m^2 matches results in [10]. Fig. 7 and Table I illustrate the large variation in rearside irradiance corresponding to different ground materials. In addition however they illustrate variations in irradiance measured by the irradiance sensors versus the effective irradiance seen by the module rear. In general, results from the PV reference cell follow the module rear effective irradiance more closely than those of the thermopile pyranometer. For example for light sand all the values are within 2.0%, while for white sand the pyranometer value is 6.6% below the module and the reference cell value matches the module. As another example, for wet soil all the values are very close, while for dry soil the reference cell matches the module to 2.6% compared to 11.4% for the pyranometer. Table I shows the root mean square of the differences between each irradiance sensor and the module for all nine materials – 3.6 W/m^2 and 16.5 W/m^2 for the reference cell and pyranometer, respectively – which illustrates the order of magnitude of the effects.

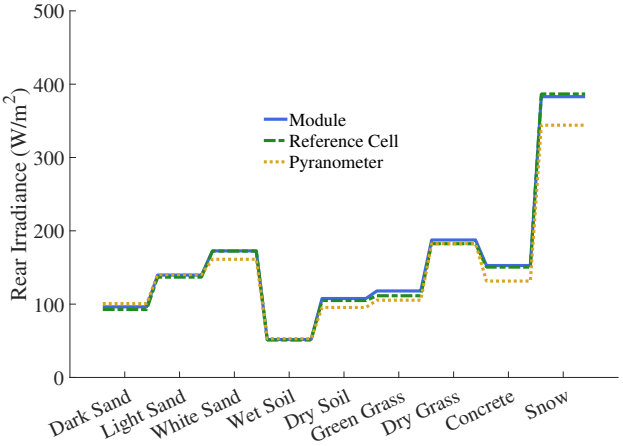

Fig. 7. Simulated rearside irradiance measured with PV reference cell and thermopile pyranometer compared with effective irradiance seen by rearside of bifacial PV module. Data are listed in Table I.

Material	Module W/m^2	Ref. Cell W/m^2	Diff. W/m^2	Pyr. W/m^2	Diff. W/m^2
Dark Sand	96.3	92.7	-3.6	100.8	4.4
Light Sand	139.6	136.8	-2.8	140.3	0.7
White Sand	172.6	172.4	-0.3	161.2	-11.4
Wet Soil	51.8	51.0	-0.7	52.9	1.1
Dry Soil	107.7	104.9	-2.7	95.4	-12.2
Green Grass	118.0	111.4	-6.6	105.4	-12.6
Dry Grass	187.5	182.4	-5.1	182.5	-5.0
Concrete	152.7	150.5	-2.1	131.5	-21.2
Snow	383.0	386.7	3.7	344.1	-38.9
Root mean square			3.6		16.5

TABLE I
SIMULATED REARSIDE IRRADIANCE DATA

Although the results presented in Fig. 7 and Table I correspond only to one set of conditions, sensors, module, and ground materials, they illustrate the types and range of effects that can arise from ground surface spectral reflectance and the potential impact on monitoring of bifacial systems using rearside irradiance measurements.

One approach to minimizing the impact of ground surface spectral reflectance on rearside irradiance monitoring is to perform spectral mismatch corrections for the selected irradiance sensors in comparison to the PV modules. However, seasonal effects that cause ground surface variation – such as variation between dry grass and green grass – may still degrade the correlation between measured irradiance and module performance if not explicitly considered.

IV. OTHER FACTORS

A. Angular Response

In addition to spectral effects, the varying sensitivity of irradiance sensors and PV modules to the angular distribution of incident radiation could also have an impact on albedo and relative irradiance measurements. Thermopile pyranometers typically have a near-cosine angular sensitivity, while PV modules and reference cells have a response that falls off faster than cosine at large incidence angles due to reflection from the air-glass-PV interfaces.

For rearside irradiance measurement, this effect should be expected to be minimal since the irradiance reaching the module rearside is primarily diffuse and normally does not have significant contribution from high incidence angles. In addition, when comparing PV reference cells to bifacial PV modules the impact of incident radiation angular distribution should be almost identical since PV modules and cells have similar angular sensitivity.

For albedo measurements angular sensitivity may be more of a concern particularly for measurement of incident radiation from the sky, which has a high direct beam component on clear days. In this case the angular sensitivity exhibited by PV reference cells may result in lower relative irradiance readings in the early morning and late afternoon due to sun angle. However, this effect can also be corrected by employing multiple reference cells to determine the direct and diffuse irradiance separately [12] [13] and in the process the angular sensitivity can be removed [14].

B. Spectral Response Variations

In order to explore the potential sensitivity of the results presented in Fig. 5 and Fig. 7 to variations in the spectral response of the PV devices, we have repeated the simulations for various combinations of spectral responses for the PV reference cell and bifacial module. As a first step, we performed the simulation for each of the six commercial bifacial PV modules whose data are reported in [9]. This yielded results very similar to those in Fig. 5 and Fig. 7. One of the features observed in [9] is that five of the bifacial modules have poorer short-wavelength response on the rear than on the front, while one has equal rear and front response. Front and rear spectral responses were also reported to be equal in [15]. Therefore we repeated the simulations using the front side responses for both front and rear, which would represent an improvement in the

module technology. This yielded results in which the PV reference cell tracked the module significantly better than shown in Fig. 5 and Fig. 7, with only approximately half the range of variation, but no significant change for the pyranometer range of variation. Finally, we repeated the simulations assuming use of a more efficient silicon PV technology for the PV reference cell, having better short and long wavelength response and therefore better matching all six PV modules of [9]. This yielded results in which the PV reference cell spectral albedo and simulated rearside irradiance measurements matched the module to within 1.5% for all ground materials.

The results of this sensitivity analysis suggest that the main factors influencing the range of variation in Fig. 5 and Fig. 7 are the widths of the PV device spectral response curves, that similar results could be expected with other typical cells and modules, and that improvement in reference cell and/or bifacial silicon module technology would likely lead to an improvement in the results presented for the reference cell, but no significant change for the pyranometer results. This last point arises simply from the differences in technology: thermopile pyranometers are designed to be broadband and spectrally insenstive, while PV reference cells are designed to have spectral sensitivity similar to PV modules.

However, our results of course only apply to mainstream crystalline silicon PV and do not apply to other PV device technologies, such as thin-film or novel materials.

V. Conclusions

Spectral effects must be considered in bifacial PV performance estimation and monitoring, due to both the strong impact of ground surface spectral reflectance on the rearside spectral irradiance available for PV power generation as well as the variability between reflectance spectra for different ground surfaces.

In addition, the impact of spectral effects should be considered when measuring both albedo and rearside irradiance. This impact depends on the choice of irradiance sensor. For our simulation examples, we found that the mismatch of spectrally responsive albedo relative to a bifacial crystalline silicon PV module varies over a range of $\pm 9.2\%$ for a thermopile pyranometer versus only $\pm 3.7\%$ for a crystalline silicon PV reference cell when considering nine different representative ground surface materials. Similarly, when comparing precited rearside irradiance measurements to the effective rearside irradiance available for PV power generation, the thermopile pyranometer and PV reference cell showed deviations versus the module on the order of 16.5 $\mathrm{W/m^2}$ versus only 3.6 $\mathrm{W/m^2}$, respectively, across the nine simulated ground surfaces. These differences arise from the fact that thermopile pyranometers are designed to be broadband and spectrally insensitive while PV reference cells are designed to match the response of PV modules.

Based on these results, spectral mismatch corrections may be needed to obtain highest accuracy in measurement and performance estimation for bifacial PV, especially when using broadband irradiance sensors.

References

[1] T. C. Russell, R. Saive, A. Augusto, S. G. Bowden, and H. A. Atwater, "The influence of spectral albedo on bifacial solar cells: A theoretical and experimental study," *IEEE Journal of photovoltaics*, vol. 7, no. 6, pp. 1611–1618, 2017.

[2] W. F. Marion, "Ground albedo measurements and modeling," *bifiPV Workshop, Denver, Colorado*, 2018. [Online]. Available: https://www.osti.gov/biblio/1569690

[3] W. F. Marion, "Albedo data for bifacial PV systems," *PV Reliability Workshop, Lakewood, Colorado*, 2019. [Online]. Available: https://www.osti.gov/biblio/1569206

[4] R. W. Andrews and J. M. Pearce, "The effect of spectral albedo on amorphous silicon and crystalline silicon solar photovoltaic device performance," *Solar Energy*, vol. 91, pp. 233–241, 2013.

[5] M. Brennan, A. Abramase, R. W. Andrews, and J. M. Pearce, "Effects of spectral albedo on solar photovoltaic devices," *Solar Energy Materials and Solar Cells*, vol. 124, pp. 111–116, 2014.

[6] R. Bird and C. Riordan. [Online]. Available: https://www.nrel.gov/grid/solar-resource/spectral.html

[7] C. Gueymard, "SMARTS: Simple model of the atmospheric radiative transfer of sunshine." [Online]. Available: https://www.nrel.gov/grid/solar-resource/smarts.html

[8] *CM21 Instruction Manual*. Kipp and Zonen, 2004.

[9] W. Herrmann, M. Schweiger, and J. Bonilla, "Performance characteristics of bifacial PV modules and power labeling," *bifiPV Workshop, Konstanz, Germany*, 2017. [Online]. Available: http://bifipv-workshop.com

[10] C. Monokroussos, Q. Gao, X. Zhang, E. Lee, Y. Wang, C. Zou, L. Rimmelspacher, J. B. Castro, M. Schweiger, and W. Herrmann, "Rearside spectral irradiance at 1 sun and application to bifacial module power rating," *Progress in Photovoltaics: Research and Applications*, 2020.

[11] B. Marion, S. MacAlpine, C. Deline, A. Asgharzadeh, F. Toor, D. Riley, J. Stein, and C. Hansen, "A practical irradiance model for bifacial PV modules," in *2017 IEEE 44th Photovoltaic Specialist Conference (PVSC)*. IEEE, 2017, pp. 1537–1542.

[12] D. Faiman, D. Feuermann, and A. Zemel, "Site-independent algorithm for obtaining the direct beam insolation from a multipyranometer instrument," *Solar Energy*, vol. 50, no. 1, pp. 53–57, 1993.

[13] B. Marion, "Multi-pyranometer array design and performance summary," in *Proc. of 1998 American Solar Energy Annual Conf*, 1998, pp. 14–17.

[14] M. Gostein, B. Stueve, R. Clark, P. Keelin, M. Grammatico, and M. Reusser, "Field trial of met station using PV reference cells," in *2020 IEEE 47th Photovoltaic Specialist Conference (PVSC)*, 2020, in preparation.

[15] J. Lopez-Garcia, A. Casado, and T. Sample, "Electrical performance of bifacial silicon PV modules under different indoor mounting configurations affecting the rear reflected irradiance," *Solar Energy*, vol. 177, pp. 471–482, 2019.